J. Am. Soc. Mass Spectrom. (2017) 28:1182–1191
DOI: 10.1007/s13361-017-1624-0

RESEARCH ARTICLE

On the SIMS Ionization Probability of Organic Molecules

Nicholas J. Popczun,[1] Lars Breuer,[1] Andreas Wucher,[2] Nicholas Winograd[1]

[1]Department of Chemistry, The Pennsylvania State University, 104 Chemistry Building, University Park, PA 16802, USA
[2]Fakultät für Physik, Universität Duisburg-Essen, 47048, Duisburg, Germany

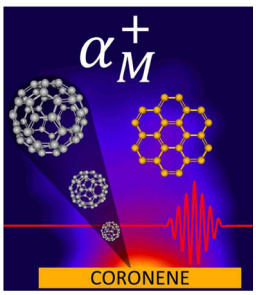

Abstract. The prospect of improved secondary ion yields for secondary ion mass spectrometry (SIMS) experiments drives innovation of new primary ion sources, instrumentation, and post-ionization techniques. The largest factor affecting secondary ion efficiency is believed to be the poor ionization probability (α^+) of sputtered material, a value rarely measured directly, but estimated to be in some cases as low as 10^{-5}. Our lab has developed a method for the direct determination of α^+ in a SIMS experiment using laser post-ionization (LPI) to detect neutral molecular species in the sputtered plume for an organic compound. Here, we apply this method to coronene ($C_{24}H_{12}$), a polyaromatic hydrocarbon that exhibits strong molecular signal during gas-phase photoionization. A two-dimensional spatial distribution of sputtered neutral molecules is measured and presented. It is shown that the ionization probability of molecular coronene desorbed from a clean film under bombardment with 40 keV C_{60} cluster projectiles is of the order of 10^{-3}, with some remaining uncertainty arising from laser-induced fragmentation and possible differences in the emission velocity distributions of neutral and ionized molecules. In general, this work establishes a method to estimate the ionization efficiency of molecular species sputtered during a single bombardment event.

Keywords: SIMS, Ionization, Post-ionization, Sputtering, Organic, Femtosecond, SNMS, LPI, Coronene, Ionization probability

Received: 9 September 2016/Revised: 30 January 2017/Accepted: 3 February 2017/Published Online: 6 March 2017

Introduction

Secondary ion mass spectrometry (SIMS) utilizes charged primary ions to sputter material from a sample surface in the form of neutral species, electrons, and positively and negatively charged ions. These secondary ions are then separated by mass-to-charge ratio and detected to elucidate the chemical composition of the sample. The introduction of polyatomic primary ion sources that distribute the kinetic energy of the primary ion near the surface has made it possible to acquire spatial and depth information of chemical distributions within heterogeneous organic samples [1–8]. The impediment to more universal adoption of SIMS for these purposes is the inefficiency observed in the conversion from a molecule present in the sample surface to a detectable secondary molecular ion. The positive secondary ion signal for species m is described by the basic SIMS equation

$$S_m = \theta_m \eta I_p Y_{tot} \alpha_m^+ \quad (1)$$

where S_m is the measured positive secondary ion signal, θ_m is the fractional mass concentration of species m, η is an effective sampling time which includes the instrument transmission, I_p is the primary ion current, Y_{tot} is the total sputter yield, and α_m^+ is the positive ionization probability of species m [9]. It should be noted that I_p is limited by the requirement of primary ion doses, which impact less than 1% of the sample surface (static limit) when surface integrity is required, whereas θ_m is an intrinsic value of the sample, leaving η, Y_{tot}, and α^+ as areas of opportunity for improving secondary ionization efficiency. Most innovations in SIMS focus on improving instrument transmission and total sputter yield, and have only recently explored increasing the ionization probability [10–13].

Improvements in secondary ionization efficiency are commonly reported as secondary ion yields (Y_m^+), or the number of secondary ions detected per primary ion particle [11–14]. An alternative is to report the useful ion yield (UY), a value derived from the ratio of the secondary ions detected to the total molecular equivalents sputtered [15, 16]. For molecular ions

Electronic supplementary material The online version of this article (doi:10.1007/s13361-017-1624-0) contains supplementary material, which is available to authorized users.

Correspondence to: Nicholas J. Popczun; *e-mail:* nicholasp@psu.edu

M^+, the useful ion yield is the product of α_M^+ , η_M and the percentage of molecules that are sputtered intact, whereas the secondary ion yield is the product of UY, θ_M and Y_{tot}. Both secondary ion yield and useful ion yield provide indirect information about the relative α_M^+ values of different systems and are attainable without information from the molecular neutral component of the sputtered material. While the useful yield can be obtained through single ion counting and atomic force microscopy (AFM) of the sputtered crater, quantification of α_m^+ is difficult since the probability of a molecule to survive the desorption process is unknown. Therefore, experimental data regarding ionization probabilities of molecular species are rarely reported, and mostly for inorganic clusters sputtered from metal [17–25] or semiconductor [26] surfaces when so.

Increasing α_m^+ is critically important for expanding SIMS applications, as poor SIMS detection efficiency for organic molecules is generally attributed to low α_m^+ [11–14, 16, 22–24, 27–34]. A numeric α_m^+ value can be determined in principle by the direct measurement of the ionic and neutral molecule intensities. Laser post-ionization (LPI) can provide access to chemical information of the neutral component in the sputtered material [35–38]. Several different LPI techniques have been explored, including single-photon ionization (SPI), resonance enhanced multiphoton ionization (REMPI), non-resonant multiphoton ionization (NRMPI), and strong-field ionization (SFI) [39–44]. The low photon flux required for SPI allows a single pulse to sample the neutral component within the extraction volume of the spectrometer, but the accessible photon energies are insufficient to ionize most organic molecules. Our laboratory utilizes SFI since it is capable of ionizing organic molecules, and we have found that the deleterious effects of laser-induced photofragmentation are greatly reduced [45–49].

The goal of this study is to utilize LPI to estimate α^+ of an organic film derived directly from sputtered ionized and neutral molecular species. The molecule investigated is coronene ($C_{24}H_{12}$), a planar, highly symmetrical polyaromatic hydrocarbon that exhibits a strong signal increase in LPI experiments relative to SIMS. To achieve our goal, the focused ionization laser is rastered in both the horizontal and vertical directions with respect to the investigated surface in order to sample the entire detectable plume of sputtered material under conditions where the post-ionization efficiency is saturated. From this series of LPI experiments, an integrated measure of sputtered neutral molecules within the acceptance volume of the mass spectrometer is obtained. Comparison of the SIMS signal with the respective integrated neutral molecular signal allows estimating α_M^+ for the molecular ion M^+ of coronene. The method provides a measurement of the number density of neutral and ionized molecules M^0 and M^+ in the volume above the bombarded surface, which is integrated over the emission velocity distribution of the sputtered particles and limited in precision by the inability to separate sputtered neutral fragments that are photo-ionized from sputtered neutral molecules that undergo photofragmentation during the post-ionization process. Apart from possible differences between the emission velocity distributions of sputtered ions and neutrals, the ratio between the acquired secondary ion and neutral signals directly relates to the molecular ionization probability α_M^+. The method also yields a visual representation of the spatial distribution of sputtered neutral molecules within the acceptance volume of the mass spectrometer, which can be used to improve post-ionization techniques.

Experimental

Instrumentation

The time-of-flight (ToF) SIMS instrument used in these experiments has been described previously [50]. In brief, the instrument consists of a 40 keV C_{60}^+ primary ion gun (Ionoptika IOG C60-40; Ionoptika Ltd., Southampton, UK) [51], a temperature controllable sample stage, a reflectron mass spectrometer, and a microchannel plate (MCP) detector equipped with a high transmission grid above the detector surface. A voltage in excess of the extraction potential is applied to the high transmission grid to prevent gain saturation from low mass photo-ionized fragments by blocking them from reaching the detector for all experiments with the exception of the sputtered photofragmentation branching ratio experiment. During the acquisition of a TOF spectrum, the grid is pulsed to ground potential within nanoseconds to allow ions above *m/z* 60 to reach the detector. The reflectron voltage was set at 2% less than the extraction field, thereby preventing ions starting directly at the surface from being reflected and detected. In connection with the time refocusing properties of the reflectron, this setting determines an effective ion extraction volume located above the surface, henceforth referred to as the sensitive volume, from which ions can be extracted and detected as described in detail elsewhere [35]. This volume then needs to be overlapped with the laser ionization volume in order to efficiently detect sputtered neutral species. For all experiments, the ionization laser and the ion extraction voltage were fired simultaneously within nanoseconds of the end of the primary pulse. As outlined in the Supplementary Information and described in detail elsewhere [17, 35], the width of the primary ion pulse determines the lower limit of the velocity distribution integral, which characterizes the measured signals. If this width is chosen long enough, particles of all relevant emission velocities are detected and the measured signal reaches a steady state value, which does not increase with increasing pulse width any more. A measurement of the pulse width dependence of the post-ionization signal is presented in Figure S1 of the Supplementary Information, which shows that a pulse width of 2000 ns is sufficient to ensure these conditions. Therefore, we chose to use this setting in order to minimize the amount of sputtered material that is not sampled by the pulsed TOF detection scheme. As described in detail elsewhere [17, 35], the signal measured under these conditions represents the number density of the emitted particles, which is integrated over their entire velocity distribution. Since the ionization probability is related to the *flux* of sputtered ionized and neutral particles rather than their *number density*, the ion/neutral ratio resulting

from a comparison of measured secondary ion and neutral signals might in principle be influenced by differences between the emission velocity distributions of secondary neutrals and ions [23]. Unfortunately, reliable experimental data regarding the magnitude of this influence is scarce [52], and practically nonexistent for molecular species. The quantity that is relevant in this context is the average inverse emission velocity of the sputtered particles, which can in principle be determined from a measurement of their emission velocity distribution. As described in Supplementary Figure S2 and surrounding text, a published experiment performed on sputtered indium atoms [53] finds the average inverse emission velocity of secondary ions and neutrals to differ by roughly a factor two, so that in this case the ionization probability appears to be underestimated by the number density ion/neutral ratio measurement. Unfortunately, a similar measurement as performed in reference [53] is not easily possible for the sputtered molecules investigated here, since the detected molecular signals are too low to map the velocity distribution particularly of the secondary ions. The result obtained from the indium experiment, however, suggests that the influence of the flux-density correction is likely to be of the order of a factor two, which is a significant uncertainty but will not change the order of magnitude of the measured ionization probability.

Sample Preparation

Coronene films were prepared on 10 × 10 mm Si shards (Ted Pella Inc., Redding, CA) that had been ultrasonicated in hexane, isopropyl alcohol, methanol, and water for 15 min per cycle. The shards were dried via N_2 stream, attached to the sample block with Cu tape and introduced to the preparatory chamber of the instrument. An additional chamber was added to the instrument for the purpose of physical vapor deposition (PVD) of films without exposure to atmosphere. The shards are cooled by passing N_2 gas through a copper tube submerged in a Dewar containing liquid N_2. The cooled gas is then passed through a quartz crystal microbalance (QCM) in contact with the sample block. An aluminum oxide crucible containing coronene was heated resistively through a tungsten filament carrying 13 A while the silicon shards were positioned in the flux of the coronene sublimed from the crucible. Coronene films were deposited to thicknesses in excess of 200 nm, measured by the QCM.

Laser System

Laser ionization of thermally evaporated and sputtered molecules was performed with a commercially available chirped pulse amplification laser system (Coherent Legend Elite Duo, Santa Clara, CA, USA), providing 40 fs pulses of 800 nm radiation at a repetition rate of 1 kHz. The pulses are converted to mid-infrared radiation through an optical parametric amplifier (OPA) (Light Conversion TOPAS-C-HE; Vilnius, Lithuania), with wavelengths tunable from 1160 to 2580 nm. Experiments were performed at 1500 nm with a peak power of about 5×10^{14} W/cm^2 to ionize the thermally evaporated or sputtered neutral molecules. The laser beam is introduced into the analysis chamber via a CaF_2 window and directed parallel to the sample surface at an angle of 38° with respect to the primary ion beam. A 150 mm (at 587.6 nm) BK-7 focusing lens positioned outside the analysis chamber focuses the laser, such that the beam waist coincides with the location of the sensitive volume. The lens was translated in both the horizontal and vertical directions perpendicular to the direction of beam propagation in order to determine the optimal overlap with the sputtered material. In some experiments, a slit aperture was inserted before the ion extraction optics of the TOF spectrometer in order to restrict the extension of the effective ionization volume along the laser beam propagation direction to the central 600 μm within the Rayleigh range (~4 mm). Power attenuation of the laser beam was performed by increasing the temporal delay between the seed and pump pulses in the first amplification stage of the OPA. A power meter (Coherent Field Max II TO; Portland, OR, USA) was used to measure the laser power as a 30 s average. The laser intensity in the focal volume was calibrated using xenon gas, which was introduced into the analysis chamber via a controllable leak valve and exhibits a well-known photoionization behavior as a function of the laser intensity.

Depth profile experiments were performed by alternating between analytical cycles and sputter erosion cycles. Acquisition of spectra for raw LPI (laser and primary ion beam active), raw SIMS (only primary ion beam active), a gas-phase background signal (GPBG) (only laser active), and a noise background signal (neither laser nor primary ion beam active) constitutes one analytical cycle. The effective SIMS signal is the difference between the raw SIMS signal and the noise signal, whereas the effective LPI signal is the raw LPI signal minus both the GPBG and SIMS signals. The analytical cycles consisted of 10,000 primary ion pulses with a pulsed primary ion beam of 25 pA current rastered across a field of view (FoV) of 150 × 150 μm^2, while a sputter erosion cycle was carried out by switching the ion beam to DC for 3 s over a 400 × 400 μm^2 raster area with an idle time of 10 s before the next analytical cycle began. An ion fraction depth profile is then plotted as a ratio of the effective molecular SIMS and LPI signals as a function of primary ion fluence.

In order to investigate the role of laser-induced photofragmentation, gas-phase experiments were performed on thermally evaporated coronene molecules. For that purpose, a clean coronene sample was heated by wrapping the copper tube normally supplying the N_2 cooling gas to the sample holder in heating tape. The laser-ionized gas-phase species were then extracted for separation by their mass-to-charge ratio and detected.

At the beginning of each experiment, the position of the laser beam was optimized for maximum LPI signal. Owing to the fact that the laser beam is tightly focused, the effective ionization volume is significantly smaller than the extension of the volume from which post-ionized neutral particles can in principle be extracted and detected. This volume, which will in the following sections be referred to as the "detectable plume," is determined by the overlap between the plume of—either

sputtered or thermally desorbed—neutral molecules and the sensitive volume of the TOF spectrometer, with its dimension both along and perpendicular to the ion extraction axis being of the order of millimeters. Since the laser beam waist is of the order of several 10 μm, the laser beam largely undersamples the detectable plume if kept at a fixed position. In order to investigate the magnitude of the undersampling, the laser focusing lens was translated in 100 μm steps both horizontally and vertically with respect to the sample surface, and LPI spectra were recorded as a function of the laser beam position until the signal vanished. To account for possible signal loss as the experiment proceeds, for instance due to variations in laser power, the signals were measured at the optimal laser position again at the end of each experiment.

Results and Discussion

The goal of this work is to establish a method to estimate the order of magnitude of α_M^+ for an organic molecule by comparing the secondary molecular ion signal with the integrated signal of the respective neutral molecular species located in the same extraction volume through laser post-ionization. Besides the velocity distribution effect described above, there are three issues associated with this goal that require consideration. First, it has been shown that damage accrued by primary ion bombardment can cause changes in α^+ near the sample surface [36]. Therefore, the value of accumulated damage is determined and the primary ion fluence needed to generate a steady state is exceeded before beginning the α^+ experiment to ensure it is independent of transient effects. Next, the degree of photofragmentation caused by the laser post-ionization of sputtered molecular species must be accounted for. Then, the saturation intensity for strong-field photoionization of sputtered coronene must be determined, which defines the extension of the effective ionization volume sampled by the laser post-ionization as described in detail elsewhere [24, 34]. Finally, the undersampling effect described above must be accounted for by scanning the laser through the effective plume of sputtered material, thereby determining the total molecular neutral signal.

Ionization Probability Versus Primary Ion Fluence

Molecular LPI and SIMS depth profiles of coronene are presented in Figure 1a. Despite the difference in signal, both the LPI and SIMS signal follow a similar trend, exhibiting an exponential decay before reaching a state of constant degradation at a fluence of about 1×10^{13} C_{60}^+/cm^2, henceforth referred to as the critical dose and marked in blue in Figure 1. Beyond this primary ion fluence, both the LPI and SIMS signals exhibit a weak linear decrease as shown in the inset of Figure 1a. This decline can, for instance, be caused by a fluence-dependent erosion rate as found in many other organic films under bombardment with C_{60} projectiles [54–56], a notion which is supported by similar rates of decline in the LPI

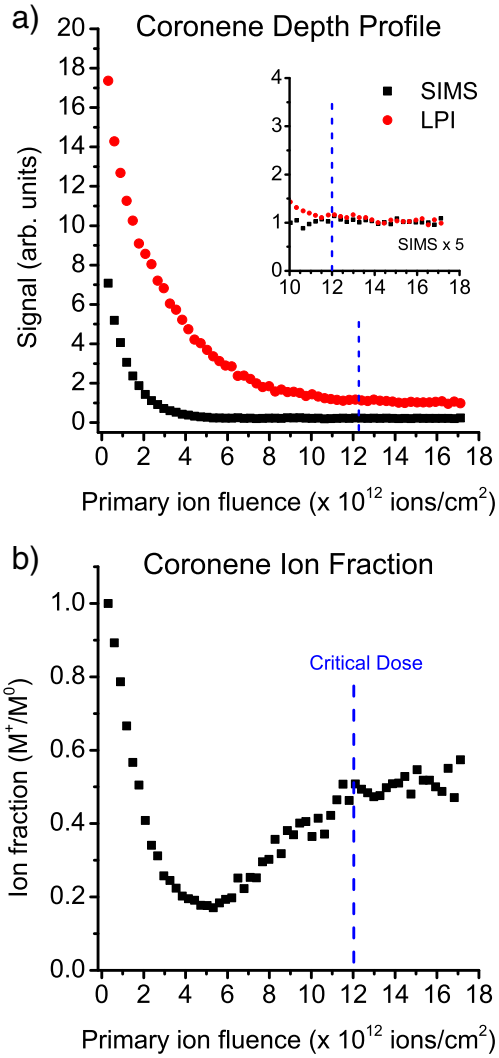

Figure 1. A coronene depth profile **(a)** showing the exponential decrease commonly observed, followed by a period of constant decline for both LPI and SIMS signals. The LPI signal is 2.5 times the SIMS signal at the clean surface, and increases to 14.4 times the SIMS signal at 5.3×10^{12} ions/cm^2. At doses above 1.2×10^{13} ions/cm^2, the LPI signal remains 4.8 ± 0.3 times the SIMS signal (inset). The coronene ion fraction **(b)** normalized to the initial ion/neutral ratio shows an early decline, after which the fraction increases until it reaches a steady state of 0.51 ± 0.02 around an ion fluence of 1.2×10^{13} ions/cm^2 (shown in blue)

(21.0% signal loss per C_{60}/nm^2) and SIMS (20.7% signal loss per C_{60}/nm^2) for primary ion fluences greater than the critical dose [57]. As a consequence, we presume that the bombardment-induced damage has reached a stationary level where the ion/neutral ratio has become independent of the primary ion fluence.

To examine the influence of bombardment-induced damage on α_M^+, the ion/neutral ratio is presented as a function of primary ion fluence in Figure 1b. It is evident that the ionization probability is strongly influenced at the beginning of the depth profile, where it at first exhibits a rather strong initial decrease

followed by a subsequent increase. This minimum in relative ionization probability corresponds to the difference in dose necessary to reach the steady state in the SIMS and LPI depth profiles, observable in Figure 1a. The relative change in α_M^+ is negative, indicating that the damage accrued with primary ion fluence suppresses SIMS ionization. Although it is possible that the initially high value of α_M^+ is due to a surface contamination, we have found that surface contamination tends to reduce the ionization probability for 20 keV C_{60}^+ primary ion bombardment of coronene and would expect similar behavior for 40 keV C_{60}^+ primary ions. In any case, the ion/neutral ratio reaches a steady state at the critical ion fluence, confirming a stationary surface state with constant α^+ at ion fluences exceeding the critical fluence.

In connection with the absolute value of the ion/neutral ratio in the steady-state region determined below, the normalized curve in Figure 1b can be used to quantitatively determine the fluence-dependent variation of the ionization probability at the beginning of the depth profile, including its value at the virgin surface being explored under static conditions. Although not further investigated here, this change in α_M^+ with bombardment-induced variations in surface composition observed for homogeneous samples might allow anticipation of matrix effects, which cause deviations from ideal behavior for heterogeneous samples [58].

Photofragmentation

The influence of photofragmentation can be described by the branching ratio, ϕ, which is defined as the probability of a neutral molecule interacting with the laser to be photo-ionized without being fragmented. This value introduces uncertainty into the measured ion/neutral ratio, since the LPI signal measured for the molecular ion may underestimate the actual number of neutral molecules interacting with the laser. The problem in quantifying the amount of photofragmentation is the difficulty to deconvolute the source of fragmentation observed during an LPI experiment. In an ideal post-ionization scenario, the laser would ionize a sputtered neutral molecule with no further laser-induced fragmentation. In this case, the branching ratio would be unity, and any detected fragment ions could be attributed solely to collision-induced fragmentation during the sputtering process. Even in that case, however, it is unlikely that all collision-induced fragments will exhibit fragmentation-free photoionization with the same efficiency as the parent molecule. In addition to the variations in chemistry of the different species, it is known that the sputtering process can cause elevated internal energy in sputtered molecules, which in turn may lead to increased photofragmentation [59]. Laser post-ionization of sputtered neutral molecular species and collision-induced fragments is therefore likely to induce further fragmentation, thereby greatly complicating the measured spectrum.

To characterize the loss of molecular coronene signal due to photofragmentation, upper and lower limits of the respective branching ratio ϕ were determined. To obtain the upper limit, a pristine coronene film was heated, and the laser was used to ionize the thermally evaporated gas-phase coronene molecules. In that case, it is safe to assume that the neutral precursor prior to photoionization and fragmentation consists only of intact coronene molecules with negligible thermal internal energy. The mass spectrum of thermally evaporated coronene (Figure 2) is dominated by six major peaks at *m/z* 300, 276, 150, 138, 100, and 92, respectively. The signals at *m/z* 300 and *m/z* 276 correspond to the molecular ion M^+ and a molecule-specific fragment $[M - C_2]^+$, which arises from the coronene molecule having evaporated a carbon dimer after internal heating during the photoionization process. Both signals are also observed in a SIMS spectrum, which shows a series of peaks corresponding to the sequential loss of carbon atoms from sputtered molecular coronene. The remaining four signals appear at *m/z* values not observed in SIMS. Instead, they arise from multiply charged M^{q+} and $[M - C_2]^{q+}$ ions with q=2 and 3, respectively. A detailed view of the LPI spectrum, shown in Supplementary Figure S3, confirms this notion, since the multiply charged species exhibit similar isotope distributions and proton loss sequences as the singly charged species. In order to determine the degree of photofragmentation, we therefore add the respective signals of all charge states and relate the resulting total $[M]^{q+}$ signal to the sum of $[M - H_n]^{q+}$, $[M - C_2H_n]^{q+}$, and all other signals appearing at *m/z* greater than *m/z* 151. The resulting branching ratio ϕ was found to be 0.53, indicating that about 53% of the thermally evaporated coronene molecules survive the SFI photoionization process intact, while the remaining 47% fragment due to the interaction with the laser, mainly by evaporative cooling via the loss of a carbon dimer.

In order to investigate photofragmentation for *sputtered* species, we look at LPI spectra (Figure 3), which were obtained under static conditions, thereby ensuring that each primary ion impacts onto a virgin surface area. Note that

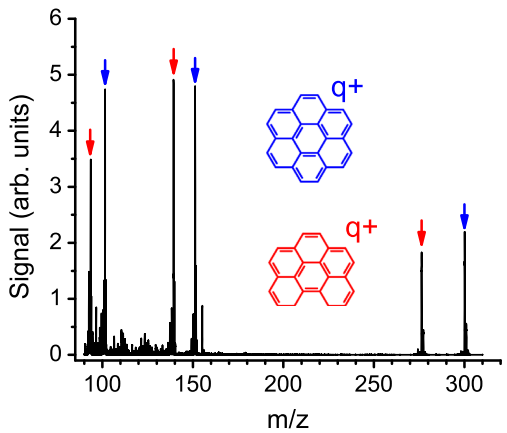

Figure 2. Strong-field ionization spectrum of thermally evaporated coronene showing the molecular ion (M^+, *m/z* 300, blue) and the characteristic fragment ion ($[M\text{-}C_2]^+$ *m/z* 276, red), as well as the signal attributed to the respective doubly and triply charged ions

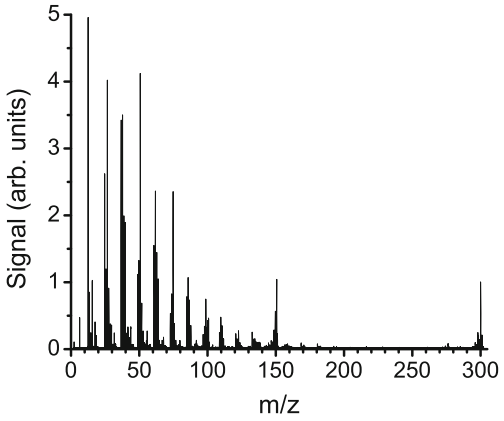

Figure 3. Laser post-ionization spectra of coronene molecules sputtered under static conditions. The ratio of singly and multiply charged molecular species (*m/z* 300) to the total signal observed is 5.1×10^{-2} for the LPI spectrum

the spectrum shown in Figure 3 was acquired with the blanking of small fragment signals as described in the Experimental section being switched off in order to detect all relevant fragment signals of all masses. Here, the calculation of ϕ is more straightforward, since the signal of $[M - C_2H_n]^+$ is small, rendering the contribution of multiply charged ions of this fragment negligible. In contrast, the signal of doubly and triply charged molecular ions at *m/z* 150 and 100 is still clearly discernible with roughly the same relative intensity as in Supplementary Figure S3. In this case, the value of ϕ is simply determined by relating the summed $[M]^{q+}$ signal to the total ion signal. As explained above, the measured spectrum reflects a convolution of laser-induced photofragmentation and photoionization of intact molecules as well as preexisting fragments that were produced in the course of the sputtering process. The resulting value of $\phi = 5 \times 10^{-2}$ therefore represents a lower bound of the photoionization branching ratio, indicating that at least 5% of the sputtered coronene molecules must survive the photoionization process intact. It should be noted, however, that this value is likely to overestimate the actual amount of photofragmentation undergone by a sputtered neutral coronene molecule. In order to examine the role of collisional fragmentation induced by the sputtering process, we look at the corresponding SIMS spectrum measured under the same bombardment conditions (Supplementary Figure S4). It is seen that this spectrum is dominated by the molecular ion peak group around *m/z* 300 and contains only small signals of low mass fragments. Assuming the ionization probability of all fragments to be similar, the data therefore indicate that the contribution of collision-induced fragmentation to the LPI spectrum of Figure 3 should be rather low.

Sampling Efficiency

The material ejected from the sample surface during a sputtering experiment fills a greater volume than the focused laser pulse required for strong-field ionization can probe in a single experiment. It is therefore necessary to characterize the undersampling of the principally detectable sputtered material to quantitatively compare the measured post-ionization signal with that measured for the respective secondary ions. The volume probed by the laser depends on the laser intensity and can be estimated from a simple barrier suppression photoionization model as described in detail elsewhere [24]. The model assumes the effective ionization volume to be defined by all points in space where the laser intensity exceeds the saturation intensity, I_{sat}, which denotes the laser intensity needed to initiate barrier suppression ionization for a selected neutral species [60]. In general, the non-linear relationship between photoionization efficiency and laser intensity, along with the spatial variation of the laser intensity overlapped with the sensitive volume of the mass spectrometer, makes calculation of the effective ionization volume complicated. In order to reduce the complexity, a slit aperture is inserted to limit the sensitive volume to the central 600 µm of the Rayleigh range in the laser propagation direction. This establishes so-called "parallel" beam conditions, where the laser intensity only depends on the radial coordinate perpendicular to the laser beam. If the laser intensity in the beam center, I_0, reaches the value of I_{sat}, saturation of the photoionization efficiency occurs, first starting in the beam center and expanding towards larger volume with increasing I_0. In the limit of high laser intensity (i.e., when $I_0 >> I_{sat}$), the measured photoion signal follows a simple relationship according to [61]

$$S(I_0) = \eta n \phi \pi l \underbrace{\left[R^2 \ln\left(\frac{I_o}{I_{sat}}\right)\right]}_{=:[R']^2} \tag{2}$$

where n is the number density of neutral molecules, l is the length of the ionization volume, and R is the distance from the beam center where the laser intensity has fallen to I_0/e [60]. The effective beam radius, R', is defined by the bracketed expression in Equation 2. A linear plot of the measured signal versus $\ln(I_0)$ therefore asymptotically follows a straight line with a slope equal to $\eta n \phi \pi l$. Extrapolation of this line to the $\ln(I_0)$ axis identifies the saturation intensity I_{sat}, [60], and the effective ionization volume is calculated as $V_i(I_0) = \pi l[R']^2$ [24].

The laser intensity calibration was examined with xenon, the photoionization signal of which was obtained in parallel with coronene, shown in Supplementary Figure S5. The experimentally measured I_{sat} value of 1.2×10^{14} W/cm^2 for Xe^+ is close to the literature value of 1.12×10^{14} W/cm^2 [61], so that no additional correction was applied to the laser intensity. The sum of the singly and multiply charged coronene signals is then plotted as a function of $\ln(I_0)$, shown in Figure 4. By extrapolating the slope of the signal increase to the horizontal axis, the saturation intensity for the coronene molecule is found to be 3.4×10^{13} W/cm^2. Using a value of $R = 27$ µm, calculated from the parameters of the unfocused beam, the effective beam radius at our setting of $I_0 = 5 \times 10^{14}$ W/cm^2 is calculated as $R' = 44$ µm.

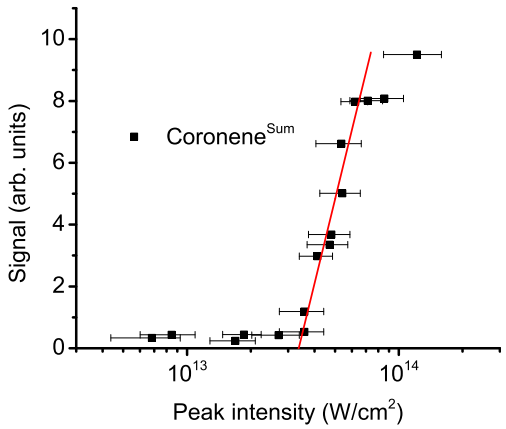

Figure 4. Sum of singly and multiply charged coronene as function of the natural log of peak laser intensity. The coronene saturation intensity was calculated to be 3.4×10^{13} W/cm^2

In order to examine the degree of undersampling, the signal measured with the laser adjusted to a certain position (typically the position delivering maximum LPI signal) must be compared with the integrated LPI signal obtained with the laser beam scanned across the entire detectable plume. With the scanning steps Δx and Δy in horizontal and vertical directions, the integral is approximated by the sum

$$S_{tot}(I_0) = \sum_{i,j} S_{ij}(I_0) \times \frac{\Delta x \Delta y}{\pi [R']^2} \qquad (3)$$

where the correction factor $v = \frac{\pi [R']^2}{\Delta x \Delta y}$ is applied in order to account for the fact that the laser samples a smaller volume $V_i = \pi l [R']^2$ than the voxel size $\Delta x \times \Delta y \times l$. For the conditions of our experiment, the factor υ was found to be 0.62. As a result, we find that the laser samples about 1.2% of the entire detectable plume of sputtered neutral molecules when adjusted to the position delivering optimum post-ionization signal. This value can be compared with the result of a similar study on indium atoms sputtered from a clean indium surface under bombardment with a 20 keV C_{60}^+ ion beam [24]. In this experiment, which was performed using the same instrument as utilized here, it was found that the laser sampled a fraction of about 3% of the detectable plume of sputtered neutral indium atoms. Since the exact value of the undersampling factor depends on the saturation intensity, the difference between both values is not surprising. The results consistently show, however, that the fraction of principally detectable post-ionized neutral particles is on the percent level and could in principle be enhanced by about two orders of magnitude if a more intense laser would be available.

Secondary Ionization Probability, α^+

In order to determine the ionization probability of a sputtered particle, it is important to note that the secondary ion spectrum measured in a SIMS experiment with delayed extraction as performed here samples all secondary ions that are present in the sensitive volume of the mass spectrometer at the time when the extraction field is switched on. For the case of the secondary ions, the experiment therefore samples the number density distribution integrated over the entire detectable plume. In principle, the spectrometer cannot distinguish between secondary ions and the corresponding photoions produced via photoionization of the respective neutral species. Therefore, if the post-ionization process would ensure that all detectable neutrals present in the sensitive volume are being ionized, the ionization probability could simply be determined from the signal ratio obtained without and with the post-ionization laser being fired. In the experiment performed here, however, the post-ionization laser is tightly focused and the undersampling effect described above must be properly accounted for. By scanning the laser through the sputtered material, we find the spatial number density distribution of post-ionized coronene molecules, which is shown in Figure 5. This figure is presented as a two-dimensional representation of the detectable plume, with the xy scanning plane oriented at an angle of 38° with respect to the primary ion beam axis. The signal plotted in Figure 5 has been normalized to the maximum LPI signal obtained with the laser set to its optimal position.

Apart from the velocity distribution correction mentioned above, the SIMS positive ionization probability is then given by the equation

$$\alpha_M^+ = \frac{M^+}{M^+ + \left(\frac{1}{\phi v}\right) \sum_{i,j} M_{ij}^0 + M^-} \qquad ,(4)$$

where M^+ represents the signal of positive molecular ions, M_{ij}^0 is the signal of post-ionized neutral molecular species measured at laser position (i,j), and M^- is the signal of negative molecular ions. Since the negative molecular coronene signal sputtered by 20 keV C_{60}^+ primary ions has been found to be much smaller

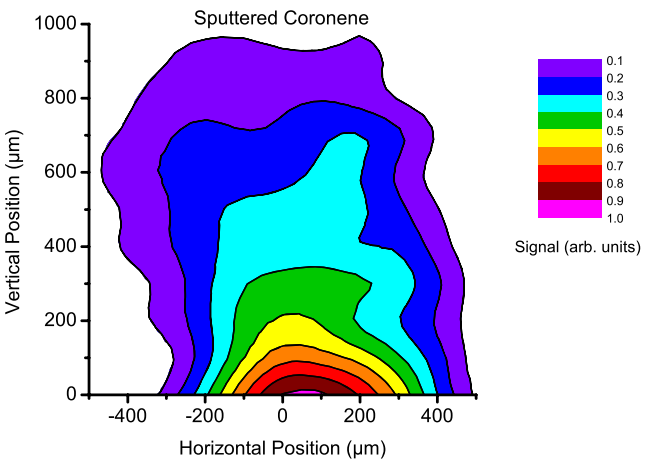

Figure 5. Two-dimensional spatial distribution of sputtered neutral coronene, normalized from 0 to 1 on the pixel of optimal laser overlap. The plane of the figure is tilted by 38° with respect to the primary ion flight path, which originates from the negative horizontal arealeft

than the total post-ionized neutral signal, shown in Supplementary Figure S6, we expect similar behavior under 40 keV C_{60}^+ primary ion bombardment and therefore have omitted M^- from the calculation in Equation 4.

The ratio of measured SIMS and LPI signals with the laser adjusted to its optimum position is 0.21, which is nearly identical to the ratio of the LPI and SIMS signals obtained from the depth profile. To calculate the true ion/neutral ratio, we sum the measured LPI signal over all 165 laser positions and apply the corrections shown in Equation 4. For a coronene surface pre-irradiated with a fluence of 40 keV C_{60}^+ primary ions greater than the critical dose at room temperature, the resulting value of α_M^+ is between 2.5×10^{-3} and 2.6×10^{-4}, depending on whether the upper or lower limit of the branching ratio ϕ is used. Note that this experiment was performed under steady state bombarding conditions, which result in damage at the sample surface that can enhance or suppress SIMS signal as seen in a section above. From the normalized data in Figure 1b, one finds that the ionization probability of intact coronene molecules sputtered from a fresh sample surface is about a factor two higher. Given the further uncertainty regarding the velocity distribution correction, we therefore conclude that the ionization probability of intact coronene molecules sputtered from a bulk coronene film under bombardment with 40 keV C_{60}^+ primary ions is of the order of 10^{-3}.

This result agrees well with the outcome of a similar experiment reported for a similar coronene film bombarded by swift heavy ions [34, 62], where the emission process is governed by electronic rather than nuclear sputtering. In principle, the technique utilized here can be transferred to other organic molecules as well, thereby providing a method to estimate relevant ionization probabilities in molecular SIMS experiments. These α^+ values are of great interest since they allow one to judge the degree of opportunity to improve the detection sensitivity in these experiments via an enhancement of the ionization probability. In that sense, what is important is the order of magnitude rather than the exact value of the ionization probability, so that the still existing ambiguity with respect to the influence of photofragmentation on one hand and possible emission velocity effects on the other hand are probably of minor importance. Nevertheless, we note that it would in principle be desirable to measure the velocity distributions of secondary ions and neutrals in the same experiment in order to account for the velocity effect. While this would be a rather straightforward task for the post-ionized neutrals, it remains extremely difficult, if not impossible, for the respective secondary ions. In the post-ionization experiment, the effective interaction volume is determined by the focused ionization laser, so that the emission velocity of the detected particles can easily be selected by the time delay between the laser pulse and a sufficiently short primary ion pulse. For the secondary ions, on the other hand, the interaction volume is determined by the entire sensitive volume of the mass spectrometer, so that the distance between the surface and the interaction volume must be significantly increased in order to achieve reasonable velocity resolution. While this has been accomplished for indium atoms that were sputtered using a 5 keV Ar^+ ion beam with several microamperes of beam current [53], it appears almost impossible for the relatively low molecular secondary ion signals obtained under C_{60}^+ cluster ion bombardment with beam currents of the order of picoamperes. Nevertheless, the method described here provides a valuable tool for comparison of molecular ionization probabilities from various sample systems, which could be used in conjunction with secondary ion yield and useful ion yield measurements to propel innovations towards enhancing the detection sensitivity in molecular SIMS.

Conclusions

The ionization probability α_M^+ of sputtered coronene molecules observed in a SIMS experiment involving 40 keV C_{60}^+ ion bombardment of a freshly prepared coronene film is estimated to be of the order of 10^{-3}. This result illuminates the magnitude by which low useful yields commonly observed in molecular SIMS experiments may be limited by poor ionization efficiency, and allows to judge prospects for possible future enhancements. More specifically, our data show that—at least for the system investigated here—there is principal headroom to increase the molecular secondary ion signal by at least two orders of magnitude using strategies targeted to enhance the ionization efficiency of the sputtered molecules.

Moreover, the results presented here show that the ionization probability changes with increasing ion fluence due to bombardment-induced variations of the chemical surface state. For a homogeneous coronene film, we find that a steady state is reached at an ion fluence around 1×10^{13} C_{60}^+/cm^2, where both the secondary ion and the post-ionized neutral signal of intact sputtered coronene molecules reach a plateau, corresponding to a constant ionization probability.

The two-dimensional spatial representation of the detectable plume illustrates the potential for improvement in post-ionization experiments. Currently, the laser post-ionization occurs in a single pass, with lens translation in the direction of laser propagation as the primary method for increasing the volume of the sputtered material that is probed by the laser. Adding additional laser passes through the sputtered material can increase the secondary neutral signal, and the two-dimensional spatial plot will be useful in guiding that development. The data also show that the post-ionization scheme applied here is in principle capable of enhancing the SIMS detection sensitivity by two or three orders of magnitude, provided a more powerful laser is used to sample the entire detectable plume of sputtered neutral particles.

Acknowledgments

The authors acknowledge the Department of Energy under grant DE-FG02-06ER15803 for the financial support of this research.

References

1. Winograd, N.: The magic of cluster SIMS. Anal. Chem. **77**, 142 A–149 A (2005)
2. Postawa, Z., Czerwinski, B., Szewczyk, M., Smiley, E.J., Winograd, N., Garrison, B.J.: Enhancement of sputtering yields due to C60 versus Ga bombardment of Ag{111} as explored by molecular dynamics simulations. Anal. Chem. **75**, 4402–4407 (2003)
3. Appelhans, A.D., Delmore, J.E.: Comparison of polyatomic and atomic primary beams for secondary ion mass spectrometry of organics. Anal. Chem. **61**, 1087–1093 (1989)
4. Wucher, A., Cheng, J., Winograd, N.: Protocols for Three-dimensional molecular imaging using mass spectrometry. Anal. Chem. **79**, 5529–5539 (2007)
5. Xu, J., Szakal, C.W., Martin, S.E., Peterson, B.R., Wucher, A., Winograd, N.: Molecule-specific imaging with mass spectrometry and a buckminsterfullerene probe: application to characterizing solid-phase synthesized combinatorial libraries. J. Am. Chem. Soc. **126**, 3902–3909 (2004)
6. Gillen, G., Roberson, S.: Preliminary evaluation of an SF5+ polyatomic primary ion beam for analysis of organic thin films by secondary ion mass spectrometry. Rapid Commun. Mass Spectrom. **12**, 1303–1312 (1998)
7. Jones, E.A., Lockyer, N.P., Vickerman, J.C.: Depth profiling brain tissue sections with a 40 keV C-60(+) primary ion beam. Anal. Chem. **80**, 2125–2132 (2008)
8. Fletcher, J.S., Rabbani, S., Henderson, A., Blenkinsopp, P., Thompson, S.P., Lockyer, N.P., Vickerman, J.C.: A new dynamic in mass spectral imaging of single biological cells. Anal. Chem. **80**, 9058–9064 (2008)
9. Vickerman, J.C., Briggs, D.: IM Publications, Chichester, UK (2013).
10. Hill, R., Blenkinsopp, P., Thompson, S., Vickerman, J., Fletcher, J.S.: A new time-of-flight SIMS instrument for 3D imaging and analysis. Surf. Interface Anal. **43**, 506–509 (2011)
11. Wucher, A., Tian, H., Winograd, N.: A mixed cluster ion beam to enhance the ionization efficiency in molecular secondary ion mass spectrometry. Rapid Commun. Mass Spectrom. **28**, 396–400 (2014)
12. Sheraz née Rabbani, S., Barber, A., Fletcher, J.S., Lockyer, N.P., Vickerman, J.C.: Enhancing secondary ion yields in time of flight-secondary ion mass spectrometry using water cluster primary beams. Anal. Chem. **85**, 5654–5658 (2013)
13. Rabbani, S., Barber, A.M., Fletcher, J.S., Lockyer, N.P., Vickerman, J.C.: TOF-SIMS with argon gas cluster ion beams: a comparison with C60+. Anal. Chem. **83**, 3793–3800 (2011)
14. Benninghoven, A., Mueller, A.: Secondary ion yields near 1 for some chemical compounds. Phys. Lett. A **40**, 169–170 (1972)
15. Deline, V.R., Katz, W., Evans, C.A., Williams, P.: Mechanism of the SIMS matrix effect. Appl. Phys. Lett. **33**, 832–835 (1978)
16. Zhang, J., Franzreb, K., Aksyonov, S.A., Williams, P.: Mass spectra and yields of intact charged biomolecules ejected by massive cluster impact for bioimaging in a time-of-flight secondary ion microscope. Anal. Chem. **87**, 10779–10784 (2015)
17. Wahl, M., Wucher, A.: VUV photoionization of sputtered neutral silver clusters. Nucl. Instrum. Methods Phys. Res. B **94**, 36–46 (1994)
18. Staudt, C., Wucher, A.: Detection of large neutral clusters in sputtering. In: Vickerman, J.C., Parks, J.E. (eds.) Resonance Ionization Spectroscopy: 9th International Symposium. AIP Press, Manchester (1998)
19. Wucher, A., Heinrich, R., Staudt, C.: In: Benninghoven, A., Bertrand, P., Migeon, H., Werner, H. (eds.) A method for quantitative determination of secondary ion formation probabilities. Proceedings of the 12th International Conference on Secondary Ion Mass Spectrometry (SIMS XII), Université Catholique de Louvain, Brussels, Belgium, September 5–10, (1999). Elsevier Science Ltd, Amsterdam, The Netherlands (2000)
20. Staudt, C., Wucher, A.: Generation of large indium clusters by sputtering. Phys. Rev. B **66**, 075419 (2002)
21. Ghalab, S., Wucher, A.: Cluster formation at metal surfaces under bombardment with (m=1, …, 5) and Ar + projectiles. Nucl. Instrum. Methods Phys. Res. B **226**, 264–273 (2004)
22. Weidtmann, B., Duvenbeck, A., Wucher, A.: Predicting secondary ion formation in molecular dynamics simulations of sputtering. Appl. Surface Sci. **255**, 813–815 (2008)
23. Mai, M., Weidtmann, B., Marpe, M., Wucher, A.: Ionization probability of sputtered indium atoms: dependence on projectile impact angle. Nucl. Instrum. Methods Phys. Res. B **317**(Part A), 130–136 (2013)
24. Breuer, L., Kucher, A., Herder, M., Wucher, A., Winograd, N.: Formation of neutral InmCn clusters under C60 ion bombardment of indium. J. Phys. Chem. A **118**, 8542–8552 (2014)
25. Samartsev, A.V., Heuser, C., Wucher, A.: Ionization probabilities of sputtered indium atoms under atomic and polyatomic Aum − ion bombardment. Surf. Interface Anal. **45**, 87–89 (2013)
26. Heinrich, R., Wucher, A.: Yields and energy distributions of sputtered semiconductor clusters. Nucl. Instrum. Methods B **140**, 27–38 (1998)
27. Fletcher, J.S., Vickerman, J.C.: A new SIMS paradigm for 2D and 3D molecular imaging of bio-systems. Anal. Bioanal. Chem. **396**, 85–104 (2009)
28. Cheng, J., Kozole, J., Hengstebeck, R., Winograd, N.: Direct comparison of Au3+ and C60+ cluster projectiles in SIMS molecular depth profiling. J. Am. Soc. Mass Spectrom. **18**, 406–412 (2007)
29. Grade, H., Winograd, N., Cooks, R.G.: Cationization of organic molecules in secondary ion mass spectrometry. J. Am. Chem. Soc. **99**, 7725–7726 (1977)
30. Nørskov, J.K., Lundqvist, B.I.: Secondary-ion emission probability in sputtering. Phys. Rev. B **19**, 5661–5665 (1979)
31. Liu, L.K., Busch, K.L., Cooks, R.G.: Matrix-assisted secondary ion mass spectra of biological compounds. Anal. Chem. **53**, 109–113 (1981)
32. Wu, K.J., Odom, R.W.: Matrix-enhanced secondary ion mass spectrometry: a method for molecular analysis of solid surfaces. Anal. Chem. **68**, 873–882 (1996)
33. Fletcher, J.S., Vickerman, J.C.: Secondary ion mass spectrometry: characterizing complex samples in two and three dimensions. Anal. Chem. **85**, 610–639 (2012)
34. Kucher, A., Wucher, A., Winograd, N.: Strong field ionization of β-estradiol in the IR: strategies to optimize molecular postionization in secondary neutral mass spectrometry. J. Phys. Chem. C **118**, 25534–25544 (2014)
35. Wucher, A.: Laser Postionization: fundamentals. In: Vickerman, J.C., Briggs, D. (eds.) TOF-SIMS: surface analysis by mass spectrometry. IM Publications, Chichester, UK (2001)
36. Willingham, D., Brenes, D.A., Wucher, A., Winograd, N.: Strong-field photoionization of sputtered neutral molecules for molecular depth profiling. J. Phys. Chem. C **114**, 5391–5399 (2010)
37. Willingham, D., Brenes, D.A., Winograd, N., Wucher, A.: Investigating the fundamentals of molecular depth profiling using strong-field photoionization of sputtered neutrals. Surf. Interface Anal. **43**, 45–48 (2011)
38. Kucher, A., Jackson, L.M., Lerach, J.O., Bloom, A.N., Popczun, N.J., Wucher, A., Winograd, N.: Near infrared (NIR) strong field ionization and imaging of C60 sputtered molecules: overcoming matrix effects and improving sensitivity. Anal. Chem. **86**, 8613–8620 (2014)
39. Levis, R.J., DeWitt, M.J.: Photoionization of polyatomic molecules using intense, near-infrared radiation of femtosecond duration. AIP Conferene Proc. 45–49 (1997).
40. Tyler, B.J., Dambach, S., Galla, S., Peterson, R.E., Arlinghaus, H.F.: Investigation of the utility of laser-secondary neutral mass spectrometry for the detection of polyaromatic hydrocarbons in individual atmospheric aerosol particles. Anal. Chem. **84**, 76–82 (2012)
41. Willey, K.F., Brummel, C.L., Winograd, N.: Photoionization mechanisms for Cr(CO)6 using high intensity laser pulses in the near-IR. Chem. Phys. Lett. **267**, 359–364 (1997)
42. Willey, K.F., Vorsa, V., Braun, R.M., Winograd, N.: Postionization of molecules desorbed from surfaces by keV ion bombardment with femtosecond laser pulses. Rapid Commun. Mass Spectrom. **12**, 1253–1260 (1998)
43. Hrubowchak, D.M., Ervin, M.H., Wood, M.C., Winograd, N.: Detection of biomolecules on surfaces using ion beam-induced desorption and multiphoton resonance ionization. Anal. Chem. **63**, 1947–1953 (1991)
44. Schuhle, U., Pallix, J.B., Becker, C.H.: Sensitive mass spectrometry of molecular adsorbates by stimulated desorption and single-photon ionization. J. Am. Chem. Soc. **110**, 2323–2324 (1988)
45. Willingham, D., Kucher, A., Winograd, N.: Strong-field ionization of sputtered molecules for biomolecular imaging. Chem. Phys. Lett. **468**, 264–269 (2009)
46. Keldysh, L.: Ionization in the field of a strong electromagnetic wave. Sov. Phys. JETP **20**, 1307–1314 (1965)

47. DeWitt, M.J., Levis, R.J.: Calculating the Keldysh adiabaticity parameter for atomic, diatomic, and polyatomic molecules. J. Chem. Phys. **108**, 7739–7742 (1998)
48. Lezius, M., Blanchet, V., Ivanov, M.Y., Stolow, A.: Polyatomic molecules in strong laser fields: nonadiabatic multielectron dynamics. J. Chem. Phys. **117**, 1575 (2002)
49. Lezius, M., Blanchet, V., Rayner, D.M., Villeneuve, D.M., Stolow, A., Ivanov, M.Y.: Nonadiabatic multielectron dynamics in strong field molecular ionization. Phys. Rev. Lett. **86**, 51–54 (2001)
50. Braun, R.M., Blenkinsopp, P., Mullock, S.J., Corlett, C., Willey, K.F., Vickerman, J.C., Winograd, N.: Performance characteristics of a chemical imaging time-of-flight mass spectrometer. Rapid Commun. Mass Spectrom. **12**, 1246–1252 (1998)
51. Weibel, D., Wong, S., Lockyer, N., Blenkinsopp, P., Hill, R., Vickerman, J.C.: A C60 primary ion beam system for time of flight secondary ion mass spectrometry: its development and secondary ion yield characteristics. Anal. Chem. **75**, 1754–1764 (2003)
52. Wucher, A.: Formation of atomic secondary ions in sputtering. Appl. Surf. Sci. **255**, 1194–1200 (2008)
53. Mazarov, P., Samartsev, A.V., Wucher, A.: Determination of energy-dependent ionization probabilities of sputtered particles. Appl. Surf. Sci. **252**, 6452–6455 (2006)
54. Shard, A.G., Brewer, P.J., Green, F.M., Gilmore, I.S.: Measurement of sputtering yields and damage in C60 SIMS depth profiling of model organic materials. Surf. Interface Anal. **39**, 294–298 (2007)
55. Gillen, G., Batteas, J., Michaels, C.A., Chi, P., Small, J., Windsor, E., Fahey, A., Verkouteren, J., Kim, K.J.: Depth profiling using C60+ SIMS—deposition and topography development during bombardment of silicon. Appl. Surf. Sci. **252**, 6521–6525 (2006)
56. Fisher, G.L., Dickinson, M., Bryan, S.R., Moulder, J.: C60 sputtering of organics: a study using TOF-SIMS, XPS, and nanoindentation. Appl. Surf. Sci. **255**, 819–823 (2008)
57. Wucher, A.: A simple erosion dynamics model of molecular sputter depth profiling. Surf. Interface Anal. **40**, 1545–1551 (2008)
58. Shard, A.G., Spencer, S.J., Smith, S.A., Havelund, R., Gilmore, I.S.: The matrix effect in organic secondary ion mass spectrometry. Int. J. Mass Spectrom. **377**, 599–609 (2015)
59. Wucher, A., Staudt, C., Neukermans, S., Janssens, E., Vanhoutte, F., Vandeweert, E., Silverans, R.E., Lievens, P.: On the internal energy of sputtered clusters. New J. Phys. **10**, 103007 (2008)
60. Hankin, S.M., Villeneuve, D.M., Corkum, P.B., Rayner, D.M.: Nonlinear ionization of organic molecules in high intensity laser fields. Phys. Rev. Lett. **84**, 5082–5085 (2000)
61. Hankin, S.M., Villeneuve, D.M., Corkum, P.B., Rayner, D.M.: Intense-field laser ionization rates in atoms and molecules. Phys. Rev. A **64**, 013405 (2001)
62. Breuer, L., Meinerzhagen, F., Herder, M., Bender, M., Severin, D., Lerach, J.O., Wucher, A.: Secondary ion and neutral mass spectrometry with swift heavy ions: organic molecules. J. Vac. Sci. Technol. B **34**, 03H130 (2016)